Optical Materials: X 12 (2021) 100104

Contents lists available at ScienceDirect

Optical Materials: X

journal homepage: www.journals.elsevier.com/optical-materials-x

# (INVITED) Opposing effects of energy migration and cross-relaxation on surface sensitivity of lanthanide-doped nanocrystals

Jingyue Fan [a], Liangliang Liang [a], Yuyang Gu [a], Xiaogang Liu [a,b,*]

[a] Department of Chemistry, National University of Singapore, 117543, Singapore
[b] SZU-NUS Collaborative Innovation Centre for Optoelectronic Science & Technology, Institute of Microscale Optoelectronics, Shenzhen University, Shenzhen 518060, China

ARTICLE INFO

*Keywords:*
Lanthanide-doping
Nanocrystal
Cross-relaxation
Energy migration
Surface sensitivity

ABSTRACT

Surface sensitivity of lanthanide-doped nanocrystals has a great utility in controlling their optical properties. Surface sensitivity can be principally promoted by energy migration. Herein, we demonstrate that cross-relaxation between lanthanides makes nanocrystals less sensitive to environmental changes. We show that by codoping ytterbium ions ($Yb^{3+}$) and neodymium ions ($Nd^{3+}$) in hexagonal-phase sodium yttrium fluorides, surface sensitivity can be manipulated by energy transfer from $Yb^{3+}$ to $Nd^{3+}$. These findings enhance our understanding of surface quenching of nanocrystals and offer new opportunities in developing highly luminous nanoprobes for molecular sensing and biomedical applications.

## 1. Introduction

For lanthanide-doped nanocrystals, rich 4*f* energy levels result in intense energy cross-talk between adjacent ions [1]. Energy transfer between identical lanthanide ions is dominated by cross-relaxation and energy migration, especially in situations involving many energy transfer steps [2–4]. Besides the crystallinity of host lattice environment, energy transfer processes dictate optical properties of lanthanide-doped nanocrystals, such as brightness, lifetime, and surface sensitivity [5–16]. Surface sensitivity is a decisive factor contributing to the development of ultrasmall, highly luminescent nanoprobes for molecular sensing [17–21]. Previous studies have reported that energy migration in nanoprobes can be an essential channel for surface sensitivity enhancement. For example, the use of gadolinium ions ($Gd^{3+}$) as migrators in organic dye-coupled nanoparticles can extend the critical distance of Förster resonance energy transfer (FRET) to 30 nm [22]. Moreover, energy migration in nanoparticles can enable single-molecule detection owing to enhanced energy transfer from terbium ($Tb^{3+}$) to surface-tethered dye molecules [23]. Unlike energy migration, cross-relaxation induces nonradiative dissipation of excitation energy within a short distance. However, the effect of cross-relaxation on nanocrystal surface sensitivity has not been investigated, even though cross-relaxation is a common example of energy transfer for many lanthanides [10,12,24].

Herein, we demonstrate that cross-relaxation suppresses the surface sensitivity of lanthanide-doped nanocrystals. Given that intense cross-relaxation hinders interactions of excited states with the surrounding surface environment, we hypothesize that surface modification or different solvents will minimally affect the luminescence profiles of nanocrystals, such as lifetime decay and photoluminescence intensity.

## 2. Results and discussion

To validate our hypothesis, we first prepared two types of lanthanide-doped β-$NaYF_4$ nanocrystals (Fig. 1a; Supplementary Figs. 1 and 2). One is $NaYF_4$@$NaYF_4$:Yb and the other is $NaYF_4$@$NaYF_4$:Nd. Notably, an inert 15-nm $NaYF_4$ core was used to minimize the effect of nanocrystal size on luminescence [25] (Fig. 1b and c; Supplementary Fig. 3). Considering that the rates of cross-relaxation and energy migration depend on interionic distances [26,27], we used two doping concentrations of $Yb^{3+}$ and $Nd^{3+}$ (each with 4% and 40%), with averaged interionic distances of 1.209 and 0.561 nm, respectively.

We first investigated the optical features of ligand-free nanocrystals dispersed in water and oleic acid-coated nanocrystals dispersed in cyclohexane. Notably, water molecules in contact with nanocrystal surfaces feature an intense *O*–H vibrational harmonic band (at 972 nm) which significantly quenches lanthanide luminescence (Supplementary Fig. 4) [7,28]. On the other hand, the oleic acid coating serves as a thin

* Corresponding author. Department of Chemistry, National University of Singapore, 117543, Singapore.
*E-mail address:* chmlx@nus.edu.sg (X. Liu).

https://doi.org/10.1016/j.omx.2021.100104
Received 17 June 2021; Received in revised form 6 October 2021; Accepted 7 October 2021
Available online 11 October 2021

passivation layer (~1 nm thick), and cyclohexane molecules feature weakly vibrational harmonic bands. As expected, we observed an increase in luminescence intensity and lifetime in the cyclohexane group compared with the ligand-free group (Fig. 1d–k). Specifically, $Yb^{3+}$-doped (40%) nanocrystals showed a much greater increase in emission lifetime (91.4% vs. 14.1%) and luminescence intensity (25.5 times vs. 3.5 times) in cyclohexane compared with their less $Yb^{3+}$-doped (4%) counterparts (Fig. 1d–g). This can be attributed to enhanced energy migration at a high $Yb^{3+}$ concentration, which promotes interactions of excited states with the surrounding surface environment. By comparison, $Nd^{3+}$-doped (40%) nanocrystals showed a much smaller increase in emission lifetime (13.9% vs. 23.8%) and luminescence intensity (1.8 times vs. 4.7 times) in cyclohexane compared with their less $Nd^{3+}$-doped (4%) counterparts (Fig. 1h–k). This can be ascribed to intense cross-relaxation at a high $Nd^{3+}$ concentration, which dissipates excitation energy locally and hinders interactions of excited states with the surface environment. Such observation was verified by a similar set of experiments in which ligand-free nanocrystals were dispersed in normal water ($H_2O$) and deuterated water ($D_2O$) (Supplementary Figs. 4 and 5) [7]. Results confirm that highly $Yb^{3+}$-doped systems promote surface sensitivity due to enhanced energy migration, whereas highly $Nd^{3+}$-doped systems reduce surface sensitivity due to enhanced cross-relaxation.

Although both energy migration and cross-relaxation lead to concentration quenching, the passivation effect of an inert shell on cross-relaxation-induced concentration quenching is small. We first ascertained the occurrence of concentration quenching in two types of nanocrystals: $NaYF_4$@$NaYF_4$:Yb and $NaYF_4$@$NaYF_4$:Nd. As shown in Fig. 2a, emission lifetimes of both $Nd^{3+}$-doped nanocrystals and $Yb^{3+}$-doped nanocrystals decrease with increased dopant concentration $x$ ($x$ = 0.1–100%), and they can be well fitted by a FRET-type quenching model:

$$\tau(x) \approx \frac{1}{1 + (x/x_o)^2} \tag{1}$$

where $\tau(x)$ is the normalized emission lifetime and $x_o$ is the critical doping concentration. When exceeding 8% doping (or 2% for $Nd^{3+}$ doping), luminescence intensity decreases after reaching a maximum, owing to the dominant effect of concentration quenching over the intensity increase in absorbance (Fig. 2b and c; Supplementary Fig. 6). Interestingly, a second turning point occurs at around 40%, caused by plateaued lifetimes after 40% doping and the continually increased absorbance:

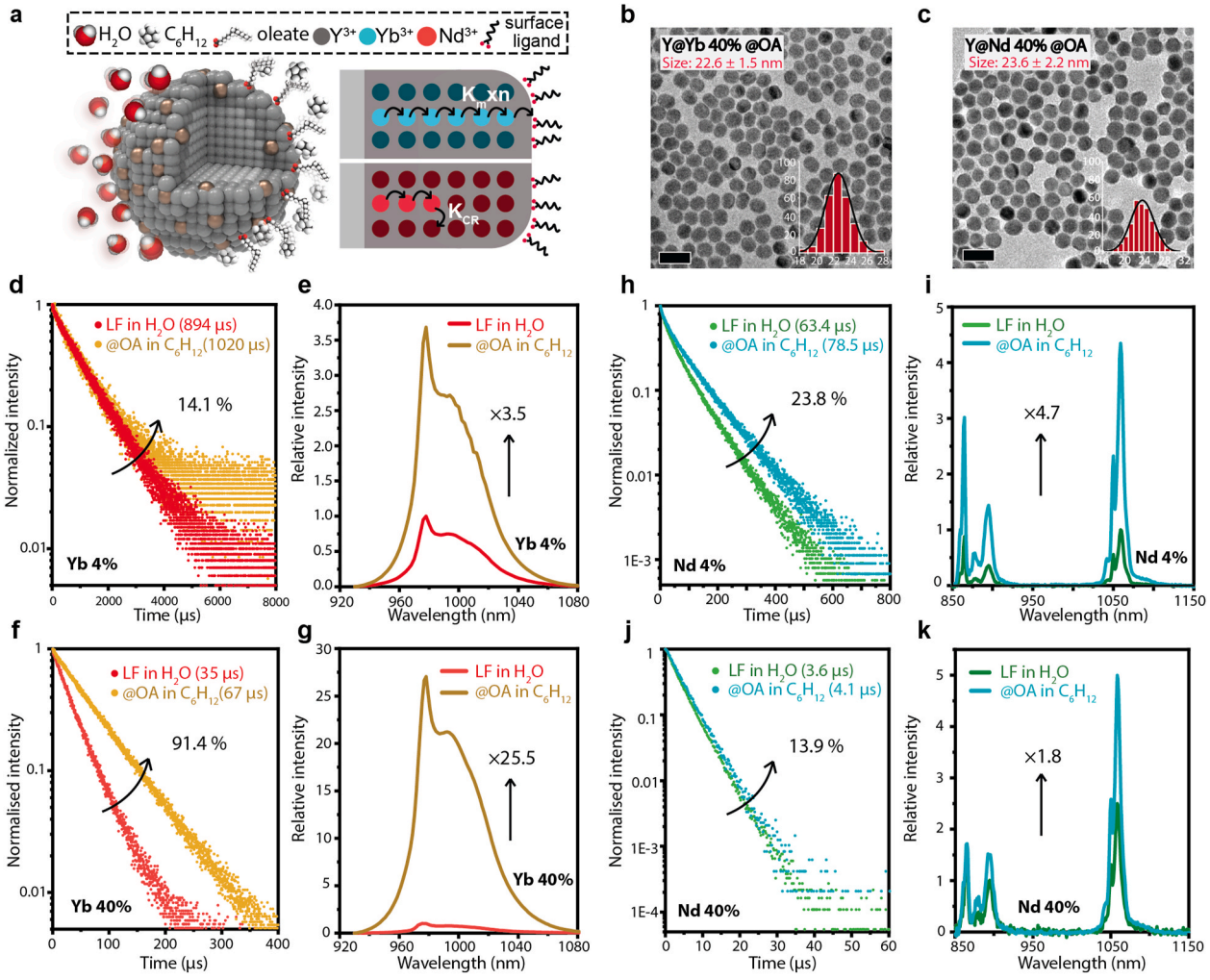


**Fig. 1.** Transmission electron microscopy (TEM) characterization and spectroscopic responses of $Nd^{3+}$- or $Yb^{3+}$-doped nanocrystals in water and cyclohexane. (a) Schematic of lanthanide-doped $NaYF_4$ nanocrystals in water and cyclohexane media and major energy transfer processes in $Nd^{3+}$-doped and $Yb^{3+}$-doped lattices. $K_m$ stands for energy migration; $K_{CR}$ stands for cross-relaxation. (b and c) TEM characterization of $NaYF_4$@$NaYF_4$:Yb(40%)@OA and $NaYF_4$@$NaYF_4$:Nd(40%)@OA nanocrystals (OA: oleate). Nanocrystal sizes are averaged over 300 measurements. Scale bars are 50 nm. (d–g) Luminescence lifetime decay profiles (d and f) and luminescence spectra (e and g) of purely $Yb^{3+}$-doped nanocrystals under 980 nm excitation. (h–k) Luminescence lifetime decay profiles (h and j) and luminescence spectra (i and k) of purely $Nd^{3+}$-doped nanocrystals under 808 nm excitation (LF: ligand-free).

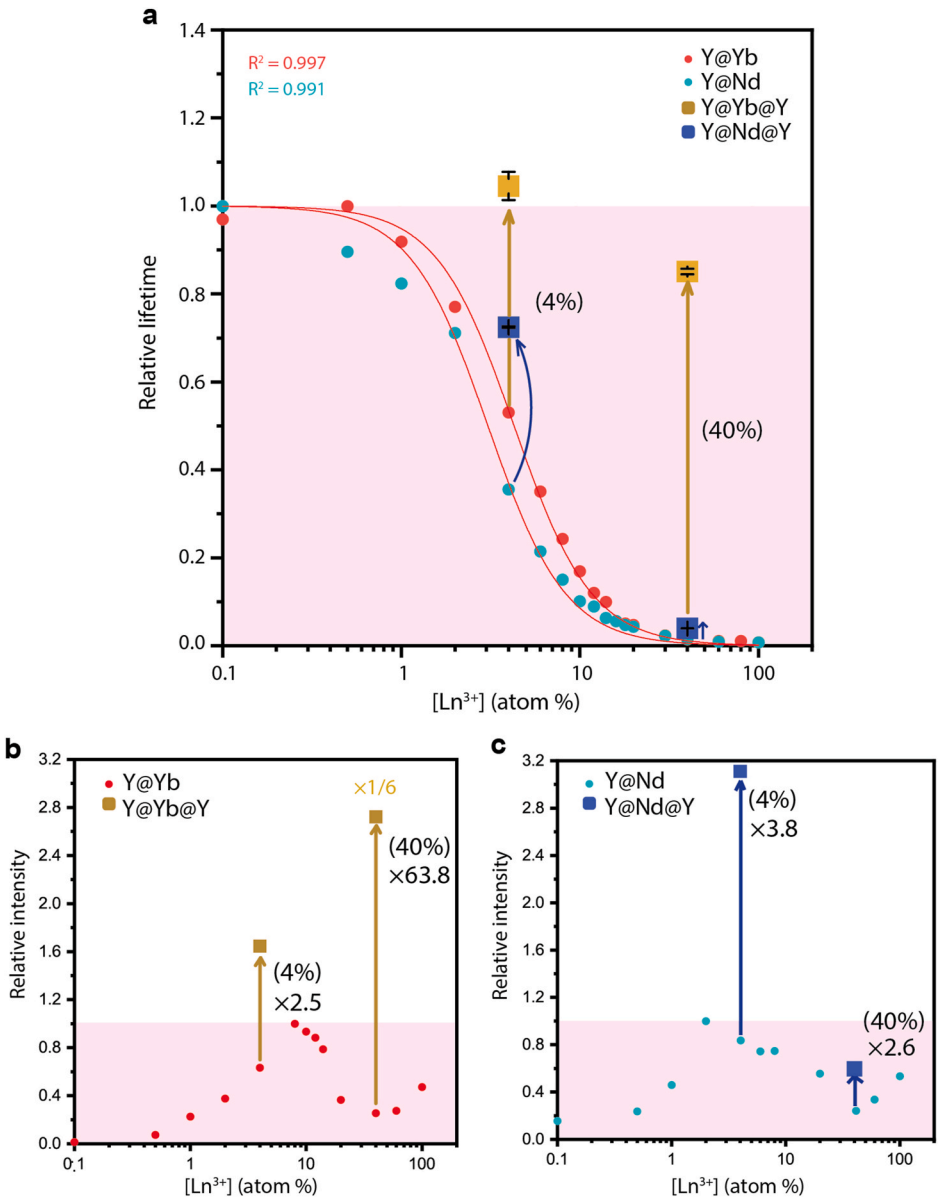


**Fig. 2.** Shell passivation and dopant concentration dependence of decay lifetime and luminescence intensity for $Nd^{3+}$- or $Yb^{3+}$-doped nanocrystals. (a) The inert shell passivation effect on lanthanide luminescence lifetime. (b and c) Shell passivation effects on the lanthanide luminescence intensity of $Yb^{3+}$- and $Nd^{3+}$-doped nanocrystal, respectively. Y@Yb, Y@Nd, Y@Yb@Y, and Y@Nd@Y denote $NaYF_4$@$NaYF_4$:Yb, $NaYF_4$@$NaYF_4$:Nd, $NaYF_4$@-$NaYF_4$:Yb@$NaYF_4$, and $NaYF_4$@$NaYF_4$:Nd@$NaYF_4$, respectively. Lifetimes in (a) are both fitted with the logistic function Eq. (1).

$$I(x) \approx k \times abs.(x) \times \tau(x) \quad (2)$$

where $I(x)$ is the normalized luminescence intensity, $abs.(x)$ is the normalized absorbance, and $k$ is the normalization constant. There is a general notion that epitaxial growth of an inert $NaYF_4$ shell reduces surface quenching [8,29]. To study the passivation effect, we coated a layer of $NaYF_4$ onto nanocrystals and measured their optical features. The increase in emission lifetime and luminescence intensity was significant upon shell passivation for 40% $Yb^{3+}$-doped nanoparticles (Fig. 2a and b), but only minimal for 40% $Nd^{3+}$-doped nanoparticles (Fig. 2a and c). Moreover, the passivation effect on 40% $Nd^{3+}$-doped nanoparticles was less than their 4% $Nd^{3+}$-doped counterparts (Fig. 2c). Short-ranged dissipation of excitation energies inhibits interactions of excited states with the surrounding environment, leading to reduced surface sensitivity toward the passivation.

To shed more light on energy transfer mechanisms that underlie surface sensitivity, we performed Monte Carlo simulations of excitation energy migration and used migration distance $d_m$ as an indicator for surface sensitivity: longer migration distances represent greater surface sensitivity. Specifically, the energy migration processes in $NaYF_4$@-$NaYF_4$:Yb and $NaYF_4$@$NaYF_4$:Nd nanocrystals are modeled as random walks on an infinite 3D lattice with weighted probabilities of moving or stopping. Our simulations reveal that at a high doping concentration (40%), the excitation energy of $Nd^{3+}$ travels a much shorter migration distance than that of $Yb^{3+}$ (Fig. 3a). Furthermore, the migration distance of excitation energies on $Yb^{3+}$-doped lattice increased with the doping concentration (Fig. 3b). In contrast, the migration distance first increased then decreased for $Nd^{3+}$-doped lattice (Fig. 3c). The shorter migration distance for 40% $Nd^{3+}$-doped lattice correlates with the reduced surface sensitivity of 40% $Nd^{3+}$-doped nanocrystals. The suppression of surface sensitivity for highly doped $Nd^{3+}$-nanosystems can be partially ascribed to the shortened migration distance of the excitation energy.

To characterize the effect of the interplay between energy migration rate $k_m$ and cross-relaxation rate $k_{cr}$ on the surface sensitivity of $Nd^{3+}$-doped nanocrystals, we calculated the transverse probability $P_{transverse}$ for excitation energy migration on $Nd^{3+}$-doped lattice at different $k_{cr}/k_m$ ratios. A larger $P_{transverse}$ represents a higher probability for excited states to interact with the surface environment, indicating greater surface sensitivity. Specifically, based on transmission electron microscope characterization, the doped shell is 3 nm thick on average. The

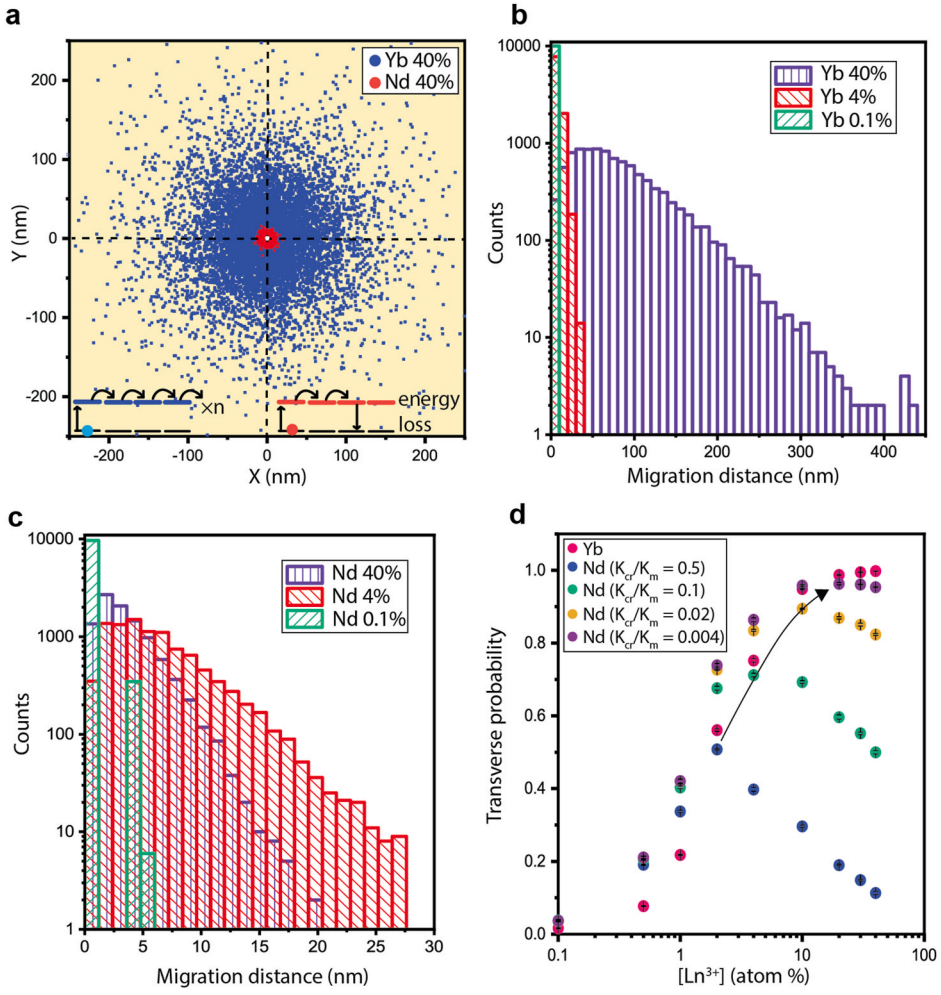


**Fig. 3.** Cross-relaxation-controlled migration by Monte Carlo simulation. (a) 2D representation of excitation energy migration on 40% $Yb^{3+}$-doped and 40% $Nd^{3+}$-doped lattices. (b) Migration distance distribution of excitation energy on $Yb^{3+}$ doped at three different concentrations. (c) Migration distance distribution of excitation energy on $Nd^{3+}$ doped at three different concentrations. (d) Transverse probability versus doping concentration. Based on migration distance distributions of $Nd^{3+}$ and $Yb^{3+}$, the probability for excitation energy to migrate beyond 3 nm (transverse probability) is plotted against doping concentrations. The plots of transverse probability for $Nd^{3+}$ are given with four varying $K_{cr}/K_m$ ratios to illustrate the effect of cross-relaxation on energy migration distance.

transverse probability for excitation energy to migrate beyond 3 nm can be statistically obtained from the distribution of migration distances. $Yb^{3+}$ is a typical energy migrator because of its simple two-level 4*f* electronic structure with an energy gap (~10,200 $cm^{-1}$) large enough to suppress nonradiative decay in sodium yttrium fluoride crystals ($\nu_{max}$ = 300–400 $cm^{-1}$) [1,5,11]. As $Nd^{3+}$ has denser electronic levels than $Yb^{3+}$, it can undergo cross-relaxation in addition to energy migration [30,31]. Results showed that the transverse probability increased with $Yb^{3+}$ doping concentration in a sigmoidal manner. By comparison, the transverse probability reached a maximum and then decreased with increased $Nd^{3+}$ doping concentration (Fig. 3d). Furthermore, the maximum point shifted to the region of low doping concentrations when the $k_{cr}/k_m$ ratio increased. As the $k_{cr}/k_m$ ratio approaches zero, the transverse probability approximates that of a purely migrating system such as the $Yb^{3+}$-doped lattice. The simulation agrees with the experimental observation that a migration system based on 40% $Yb^{3+}$-doped nanocrystals has greater surface sensitivity than 40% $Nd^{3+}$-doped nanocrystals (Fig. 1f–g and 1j-1k). Furthermore, the results indicate that unlike energy migration, cross-relaxation suppresses surface sensitivity by reducing the migration distance of excitation energy, shifting the maximally achievable surface sensitivity to small dopant ratios.

We further investigated optical features of nanocrystal thin films toward water desorption (Fig. 4e; Supplementary Fig. 7). Thermogravimetric analysis and Fourier-transform infrared spectroscopy indicated that thermal heating to 58 °C removed surface-adsorbed water molecules (Supplementary Fig. 7) [32,33]. As expected, $NaYF_4$:Nd/Yb (40/40%) nanocrystals showed a larger increase in emission lifetime (37.2% vs. 7.4%) and luminescence intensity (1.171 times vs. 1.076 times) toward water desorption compared with $NaYF_4$:Nd(40%) counterparts (Fig. 4a–d). The improvement in surface sensitivity can be explained by energy transfer between $Nd^{3+}$ and $Yb^{3+}$, as evidenced by the bi-exponential nature of the 864 nm decay on $Nd^{3+}$ (Supplementary Fig. 8). Because of the long lifetime of $Yb^{3+}$, its excitation energy migrates over a long distance before being transferred back to $Nd^{3+}$. Consequently, the 864 nm $Nd^{3+}$ emission is more susceptible to environmental changes.

## 3. Conclusion

In this work, we found that cross-relaxation can diminish the surface sensitivity of lanthanide-doped nanocrystals. Besides, the surface sensitivity of nanocrystals can be manipulated by balancing the level of energy migration and cross-relaxation. As a result, inert shell passivation is inessential for $Nd^{3+}$-sensitized luminescence, which boosts the development of ultrasmall upconversion nanoprobes. Since many activator ions (e.g., thulium, holmium, and erbium) in upconversion processes are also known to undergo cross-relaxation, our findings may offer insights into the development of a general upconversion nanocrystal platform for luminescence sensing.

## 4. Materials and methods

### 4.1. Materials

1-octadecene (90%), oleic acid (90%), yttrium acetate hydrate ($Y(CH_3CO_2)_3{\cdot}xH_2O$; 99.9%), ytterbium acetate hydrate (Yb

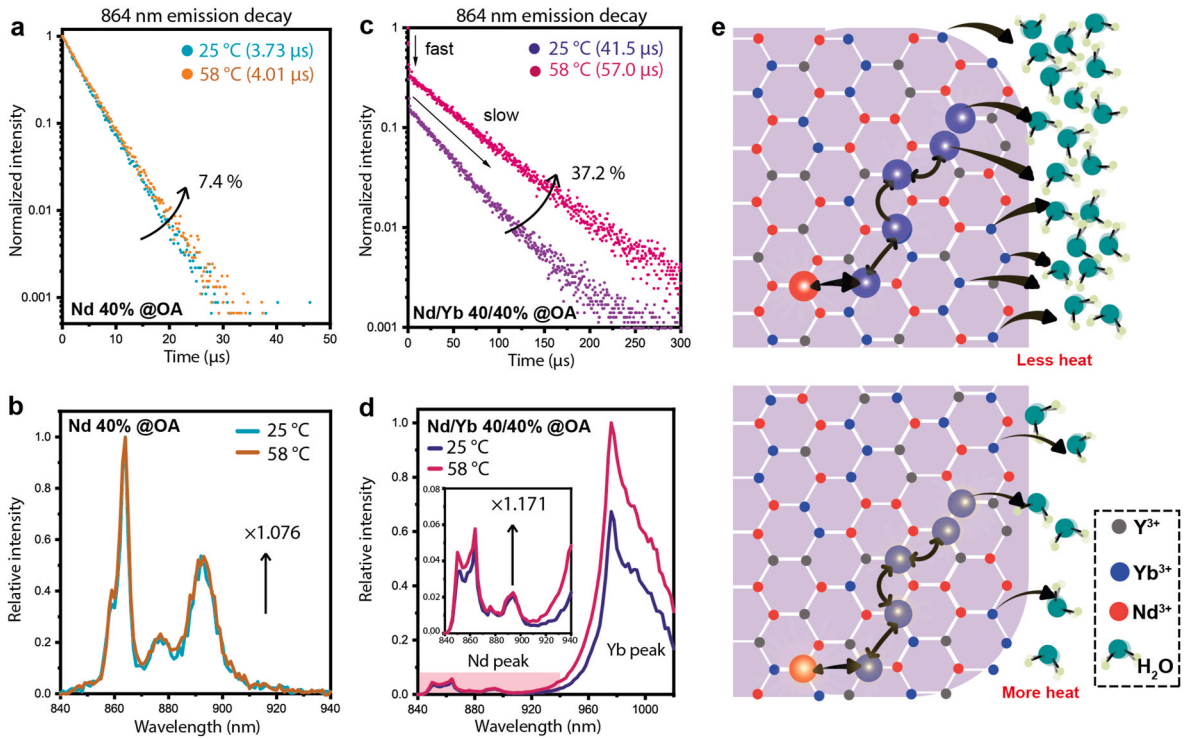


**Fig. 4.** The effect of $Yb^{3+}$ codoping on the spectroscopic response of $Nd^{3+}$ emission under heating (a and b) Luminescence decay and intensity spectra of $NaYF_4$:Nd (40%)@OA nanocrystal thin film. (c and d) Luminescence decay and spectra of codoped $NaYF_4$:Nd/Yb(40/40%)@OA nanocrystal thin film. (e) Schematic of heating effect on the codoped nanosystem. The surface ligand oleate is omitted for clarity.

$(CH_3CO_2)_3{\cdot}xH_2O$; 99.9%), neodymium acetate hydrate (Nd $(CH_3CO_2)_3{\cdot}xH_2O$; 99.9%), sodium hydroxide (NaOH; >98%), ammonium fluoride ($NH_4F$; >98%), methanol (>99%), ethanol (>99%), hydrochloric acid (37%) and cyclohexane (>99%) were all purchased from Sigma-Aldrich and used as received without further treatment.

### 4.2. Physical measurements

Powder X-ray diffraction experiments were performed on a Bruker D8 Advance diffractometer at a scanning rate of 2.4° $min^{-1}$ in a 2θ range from 10° to 80° (Cu Kα radiation, 40 kV, 40 mA, λ = 1.5418 Å). The size and morphology of the as-prepared nanocrystals were characterized using a JEOL-3010 transmission electron microscope operating at an acceleration voltage of 300 kV. UV–visible absorption spectra of the nanocrystals dispersed in cyclohexane or water were acquired using an Agilent Cary 5000 UV–Visible–NIR spectrophotometer. Luminescence spectra were recorded with an Edinburgh FLS1000 spectrofluorometer equipped with a Hamamatsu NIR photomultiplier detector (C9940-02), in conjunction with either a continuous-wave 808 nm (MDL–III–808 nm) or 980 nm diode laser (MDL–III–980 nm). In particular, the photoluminescence spectra of purely $Yb^{3+}$-doped nanocrystals were collected under microsecond pulsed excitation in time-resolved emission spectrum mode to avoid spectral contamination from the excitation source. The integrated intensity over time after pulsed excitation at emission wavelengths between 930 and 1080 nm constitutes $Yb^{3+}$ luminescence spectra. Luminescence decay curves were measured with an Edinburgh FLS1000 spectrofluorometer in multichannel scaling mode with a nanosecond Ekspla NT352 optical parametric oscillator pumped by a 3.8-ns-pulsed 10 Hz Nd:YAG laser.

Thermogravimetric analysis was done with a Discovery Thermogravimetric Analyzer. A few milligrams of air-dried solid nanocrystals were spread evenly on a ceramic pan. From 300 K to 570 K, the machine operated in ambient condition at a heating rate of 5 K/min and then undergone isothermal heating at 570 K for 10 min, followed by cooling from 570 K to 300 K at a rate of 20 K/min. The sample was heated again at 5 K/min before cooling down naturally. Fourier-transform infrared spectra were obtained using a Bruker Alpha FTIR spectrometer (with KBr pellet). Heating of drop-casted nanocrystal thin films was performed using a Minco Polyimide Thermofoil™ heater pasted underneath a glass slide and driven by a power supply unit (Agilent E3646A Programmable DC Power Supply 0–8 V, 3 A/0–20 V, 1.5 A) between 0 and 10 V at 1.5 A. Temperature variations were monitored using a FLIR ONE® digital thermal camera.

### 4.3. Synthesis of $NaYF_4$:Nd/Yb core nanocrystals

$NaYF_4$:Nd/Yb nanocrystals were synthesized via a co-precipitation method [34]. In a typical experiment, 1-octadecene (7.0 mL) and oleic acid (3.0 mL) was added to an aqueous solution (2.0 mL) of $Y(CH_3CO_2)_3$, $Yb(CH_3CO_2)_3$ and $Nd(CH_3CO_2)_3$ in a 50-mL flask at varied proportions with a total lanthanide content of 0.4 mmol. The mixture was heated in an oil bath in ambient condition at 150 °C for 1 h and then cooled to 50 °C. A methanol solution (6.0 mL) of $NH_4F$ (1.6 mmol) and NaOH (1.0 mmol) was subsequently added. After stirring for 30 min at 50 °C, the reaction was heated to 105 °C and purged by nitrogen gas for 20 min. The mixture was then heated to 290 °C and maintained at this temperature for 2 h under a nitrogen flow. After cooling to room temperature, the resulting nanocrystals were precipitated by centrifugation, purified several times with a mixture of ethanol and cyclohexane, and finally redispersed in 4.0 mL of cyclohexane.

### 4.4. Synthesis of $NaYF_4$:Nd/Yb@$NaYF_4$:Nd/Yb core-shell nanocrystals

1-Octadecene (7.0 mL) and oleic acid (3.0 mL) were added to an aqueous solution (2.0 mL) of $Y(CH_3CO_2)_3$, $Yb(CH_3CO_2)_3$ and Nd $(CH_3CO_2)_3$ in a 50-mL flask at varied proportions with a total lanthanide content of 0.4 mmol. The mixture is heated in an oil bath in ambient condition at 150 °C for 1 h and then cooled to 80 °C. The as-synthesized

core nanocrystals dispersed in cyclohexane were added. After 40 min, the resultant mixture was cooled to 50 °C. A methanol solution (6.0 mL) of $NH_4F$ (1.6 mmol) and NaOH (1.0 mmol) was subsequently added. After stirring for 30 min at 50 °C, the reaction was heated to 105 °C and purged by nitrogen gas for 20 min. The mixture was heated to 290 °C and maintained at this temperature for 2 h under a nitrogen flow. After cooling to room temperature, the resulting nanocrystals were precipitated by centrifugation, purified several times with a mixture of ethanol and cyclohexane, and finally redispersed in 4.0 mL of cyclohexane. If an additional layer of shell is desired, the above synthesis can be repeated with the as-synthesized core-shell nanocrystals.

### 4.5. Preparation of hydrophilic nanoparticles

Hydrochloric acid was used to render nanoparticles hydrophilic and dispersible in water [35]. Nanocrystals (1.0 mL, 0.1 mmol) dispersed in cyclohexane were mixed with 1.0 mL of ethanol in a 2-mL centrifuge tube. Subsequently, the mixture was centrifuged for 10 min (at 16,500 rpm). The precipitate was redispersed in a mixture of ethanol (1.0 mL) and HCl solution (1.0 mL, 0.2 M) by sonication for 10 min, after which the solution was centrifuged for 15 min at 16,500 rpm. The precipitate was redispersed in 2 mL ethanol and centrifuged for 25 min at 16,500 rpm. Ligand-free nanoparticles were finally redispersed in deionized water.

## CRediT authorship contribution statement

**Jingyue Fan:** Conceptualization, Methodology, Investigation, Formal analysis, Modeling, Writing – original draft, Visualization. **Liangliang Liang:** Methodology, Writing – review & editing, Visualization. **Yuyang Gu:** Validation, Modeling. **Xiaogang Liu:** Supervision, Writing – review & editing, Funding acquisition.

## Declaration of competing interest

The authors declare that they have no known competing financial interests or personal relationships that could have appeared to influence the work reported in this paper.

## Acknowledgements

This work was supported by Agency for Science, Technology and Research (A*STAR) under its AME program (Grant NO. A1883c0011 and A1983c0038), National Research Foundation, the Prime Minister's Office of Singapore under its NRF Investigatorship Programme (Award No. NRF-NRFI05-2019-0003), and the King Abdullah University of Science and Technology (KAUST) Office of Sponsored Research (Award No. OSR-2018-CRG7-3736).

## Appendix A. Supplementary data

Supplementary data to this article can be found online at https://doi.org/10.1016/j.omx.2021.100104.

## References

[1] G. Blasse, B.C. Grabmaier, Luminescent Materials, first ed., Springer-Verlag Berlin Heidelberg, 1994.
[2] G. Blasse, H.S. Kiliaan, A.J. De Vries, A study of the energy transfer processes in sensitized gadolinium phosphors, J. Alloys Compd. 126 (1986) 139.
[3] F. Auzel, Upconversion and anti-Stokes processes with f and d ions in solids, Chem. Rev. 104 (2004) 139.
[4] F. Wang, R. Deng, J. Wang, Q. Wang, Y. Han, H. Zhu, X. Chen, X. Liu, Tuning upconversion through energy migration in core-shell nanoparticles, Nat. Mater. 10 (2011) 968.
[5] J.F. Suyver, J. Grimm, M.K. van Veen, D. Biner, K.W. Krämer, H.U. Güdel, Upconversion spectroscopy and properties of $NaYF_4$ doped with $Er^{3+}$, $Tm^{3+}$ and/or $Yb^{3+}$, J. Lumin. 117 (2006) 1.
[6] F. Wang, X. Liu, Upconversion multicolor fine-tuning: visible to near-infrared emission from lanthanide-doped $NaYF_4$ nanoparticles, J. Am. Chem. Soc. 130 (2008) 5642.
[7] R. Arppe, I. Hyppanen, N. Perala, R. Peltomaa, M. Kaiser, C. Wurth, S. Christ, U. Resch-Genger, M. Schaferling, T. Soukka, Quenching of the upconversion luminescence of $NaYF_4$:$Yb^{3+}$, $Er^{3+}$ and $NaYF_4$:$Yb^{3+}$, $Tm^{3+}$ nanophosphors by water: the role of the sensitizer $Yb^{3+}$ in nonradiative relaxation, Nanoscale 7 (2015) 11746.
[8] N.J. Johnson, S. He, S. Diao, E.M. Chan, H. Dai, A. Almutairi, Direct evidence for coupled surface and concentration quenching dynamics in lanthanide-doped nanocrystals, J. Am. Chem. Soc. 139 (2017) 3275.
[9] T. Kushida, Energy transfer and cooperative optical transitions in rare-earth doped inorganic materials. I. Transition probability calculation, J. Phys. Soc. Japan 34 (1973) 1318.
[10] K.M. Dinndorf, Energy Transfer between Thulium and Holmium in Laser Hosts, Physics, Massachusetts Institute of Technology, 1993.
[11] Y. Mita, T. Ide, T. Katase, H. Yamamoto, Energy transfer and migration processes in $Yb^{3+}$-ion-sensitized, rare-earth-ion-activated luminescent materials, J. Lumin. 72–74 (1997) 959.
[12] W. Wei, Y. Zhang, R. Chen, J. Goggi, N. Ren, L. Huang, K.K. Bhakoo, H. Sun, T.T. Y. Tan, Cross relaxation induced pure red upconversion in activator- and sensitizer-rich lanthanide nanoparticles, Chem. Mater. 26 (2014) 5183.
[13] D.L. Dexter, J.H. Schulman, Theory of concentration quenching in inorganic phosphors, J. Chem. Phys. 22 (1954) 1063.
[14] L. Liang, X. Qin, K. Zheng, X. Liu, Energy flux manipulation in upconversion nanosystems, Acc. Chem. Res. 52 (2019) 228.
[15] X. Qin, X. Liu, W. Huang, M. Bettinelli, X. Liu, Lanthanide-Activated phosphors based on 4f-5d optical transitions: theoretical and experimental aspects, Chem. Rev. 117 (2017) 4488.
[16] X. Qin, L. Shen, L. Liang, S. Han, Z. Yi, X. Liu, Suppression of defect-induced quenching via chemical potential tuning: a theoretical solution for enhancing lanthanide luminescence, J. Phys. Chem. C 123 (2019) 11151.
[17] J. Zhou, A.I. Chizhik, S. Chu, D. Jin, Single-particle spectroscopy for functional nanomaterials, Nature 579 (2020) 41.
[18] C. Wurth, S. Fischer, B. Grauel, A.P. Alivisatos, U. Resch-Genger, Quantum yields, surface quenching, and passivation efficiency for ultrasmall core/shell upconverting nanoparticles, J. Am. Chem. Soc. 140 (2018) 4922.
[19] C. Li, L. Xu, Z. Liu, Z. Li, Z. Quan, A.A. Al Kheraif, J. Lin, Current progress in the controlled synthesis and biomedical applications of ultrasmall (<10 nm) $NaREF_4$ nanoparticles, Dalton Trans. 47 (2018) 8538.
[20] M. Quintanilla, F. Ren, D. Ma, F. Vetrone, Light management in upconverting nanoparticles: ultrasmall core/shell architectures to tune the emission color, ACS Photonics 1 (2014) 662.
[21] J.R. Lakowicz, Fluorescence Sensing and Novel Fluorophores Principles of Fluorescence Spectroscopy, Springer US, 2006, p. 623.
[22] R. Deng, J. Wang, R. Chen, W. Huang, X. Liu, Enabling forster resonance energy transfer from large nanocrystals through energy migration, J. Am. Chem. Soc. 138 (2016) 15972.
[23] J. Zhou, C. Li, D. Li, X. Liu, Z. Mu, W. Gao, J. Qiu, R. Deng, Single-molecule photoreaction quantitation through intraparticle-surface energy transfer (i-SET) spectroscopy, Nat. Commun. 11 (2020) 4297.
[24] Y. Liu, Y. Lu, X. Yang, X. Zheng, S. Wen, F. Wang, X. Vidal, J. Zhao, D. Liu, Z. Zhou, C. Ma, J. Zhou, J.A. Piper, P. Xi, D. Jin, Amplified stimulated emission in upconversion nanoparticles for super-resolution nanoscopy, Nature 543 (2017) 229.
[25] F. Wang, J. Wang, X. Liu, Direct evidence of a surface quenching effect on size-dependent luminescence of upconversion nanoparticles, Angew. Chem. Int. Ed. 49 (2010) 7456.
[26] D.L. Dexter, A theory of sensitized luminescence in solids, J. Chem. Phys. 21 (1953) 836.
[27] T. Förster, 10th Spiers Memorial Lecture. Transfer mechanisms of electronic excitation, Discuss. Faraday Soc. 27 (1959) 7.
[28] M. Stomp, J. Huisman, L.J. Stal, H.C. Matthijs, Colorful niches of phototrophic microorganisms shaped by vibrations of the water molecule, ISME J. 1 (2007) 271.
[29] S. Wen, J. Zhou, K. Zheng, A. Bednarkiewicz, X. Liu, D. Jin, Advances in highly doped upconversion nanoparticles, Nat. Commun. 9 (2018) 2415.
[30] G.H.D.a.H.M. Crosswhite, The spectra of the doubly and triply ionized rare earths, Appl. Opt. 2 (1963) 675.
[31] M.B.H.G. Danielmeyer, P. Balmer, Fluorescence quenching in Nd:YAG, Appl. Phys. 1 (1973) 269.
[32] Z. Wang, J. Christiansen, D. Wezendonk, X. Xie, M.A. van Huis, A. Meijerink, Thermal enhancement and quenching of upconversion emission in nanocrystals, Nanoscale 11 (2019) 12188.
[33] Y. Hu, Q. Shao, P. Zhang, Y. Dong, F. Fang, J. Jiang, Mechanistic investigations on the dramatic thermally induced luminescence enhancement in upconversion nanocrystals, J. Phys. Chem. C 122 (2018) 26142.
[34] F. Wang, R. Deng, X. Liu, Preparation of core-shell $NaGdF_4$ nanoparticles doped with luminescent lanthanide ions to be used as upconversion-based probes, Nat. Protoc. 9 (2014) 1634.
[35] N. Bogdan, F. Vetrone, G.A. Ozin, J.A. Capobianco, Synthesis of ligand-free colloidally stable water dispersible brightly luminescent lanthanide-doped upconverting nanoparticles, Nano Lett. 11 (2011) 835.